NJC

Accepted Manuscript

ROYAL SOCIETY OF CHEMISTRY

rsc.li/njc

View Article Online
DOI: 10.1039/C8NJ03316A

Journal Name

ARTICLE

Facile synthesis of triphenylamine and phenothiazine based Schiff bases for aggregation induced enhanced emission, white light generation, and highly selective and sensitive copper (II) sensing

Received 00th January 20xx,
Accepted 00th January 20xx

DOI: 10.1039/x0xx00000x

www.rsc.org/

Vivek Anand, Balaji Sadhasivam and Raghavachari Dhamodharan*

Two new Schiff bases, one triphenylamine based (**TPA-SB**) and another phenothiazine based (**PTz-SB**) were synthesized via facile reactions. Both the molecules showed aggregation-induced enhanced emission (AIEE) properties. In fact, a 8-fold increase in the fluorescence intensity was observed for a 20:80 THF:water mixture of **TPA-SB** as compared to that in pure THF. The AIEE nature was further confirmed by dynamic light scattering (DLS) experiment and transmission electron microscopy (TEM) studies. These two moieties were mixed with rhodamine B (**Rh-B**) dye to obtain efficient white light emission (WLE) in solution and gelatin gel phase. Excellent Commission Internationale d'Eclairage (CIE) coordinates (0.32, 0.34) and (0.31, 0.34) were obtained in the solution and gelatin gel phase, respectively. The correlated color temperatures (CCT) obtained in the two phases (6115 K in solution and 6500 K in gelatin gel) suggested that the system emitted cool white light. The mechanism of WLE as verified through fluorescence titration, lifetime and spectral overlap studies, was found to arise due to Förster resonance energy transfer (FRET) among the three fluorophores. The optical band gaps obtained from UV-visible spectroscopy were 2.82 and 2.59 eV for **TPA-SB** and **PTz-SB**, respectively. The SEM and TEM studies revealed that in the aggregted state **TPA-SB** exhibited spherical while **PTz-SB** showed nanopyramidal morphology. The new molecules were thermally robust as reflected from their TGA and DSC studies. Interestingly, **TPA-SB** showed remarkable fluorescence quenching response towards copper (II) cation with a limit of detection (LOD) value of 1.8 ppb, while **PTz-SB** showed the LOD value of 4.8 ppb. The Schiff bases were particularly selective towards Cu (II) ions without interference from ten other common cations. Hence, these easily synthesizable Schiff bases are of multiple applicability viz. AIEE, WLE and Cu^{2+} sensing.

Introduction

White light emission (WLE) from organic fluorophores (OFs) has tremendous applications owing to low-cost, lightweight, ease of synthesis and the ability to form ultrathin films.[1-6] In OFs, white light can be attained in two ways: either by the blending of different components (blue, green and red emitting materials), the fluorescence of which covers the entire visible spectrum or from a single component system.[7-10] Nevertheless, single OFs emitting white light are scarce in view of the constraints imposed by the Kasha's rule. Consequently, multi-component organic white light emitting materials are in rampant demand.[11,12] The various mechanisms, which lead to WLE in OFs are single molecular excited state intramolecular proton transfer (ESIPT),[13,14] solvent assisted self-assembly,[15,16] ESIPT coupled aggregation-induced enhanced emission (AIEE)[17,18] and Förster resonance energy transfer (FRET).[19-22] Among these, FRET involves the transfer of energy from the excited electronic state of a donor to an acceptor. The necessary conditions for FRET to take place are: significant overlap between the emission spectrum of the donor and absorption spectrum of the acceptor; and the separation between the donor and acceptor should be small.[22,23]

WLE in the solid state is always preferred over their solution phase counterparts.[24] But as a matter of fact, very few OFs give eloquent emission in solid or aggregated state owing to aggregation-caused quenching (ACQ).[25,26] The application of OFs in diverse fields has been boasted by aggregation-induced emission (AIE), discovered by Tang *et al.,* in 2001.[27] By definition, AIE is a phenomenon in which a fluorophore, weakly emitting in its dilute solution becomes highly

Department of Chemistry, Indian Institute of Technology Madras, Chennai-600036 India, E-mail: damo@iitm.ac.in
† Footnotes relating to the title and/or authors should appear here.
Electronic Supplementary Information (ESI) available: [details of any supplementary information available should be included here]. See DOI: 10.1039/x0xx00000x

View Article Online
DOI: 10.1039/C8NJ03316A

fluorescent on aggregation.[28] The phenomenon chiefly responsible for AIE behaviour is the restriction of intramolecular motion (RIM).[29]

Fused aromatic ring systems are utilized frequently as OFs for optoelectronic applications.[30,31] Utilization of simple molecules for WLE, avoiding harsh conditions is promising for various optoelectronic applications, as most of the present methods utilize either complicated synthesis or harsh conditions like high temperature, use of corrosive acids etc. Triphenylamine, for instance, apart from being one of the most efficient hole transporting materials, has excellent electronic and mechanical properties.[32-35] Furthermore, it has low ionization potential, high electron affinity and good UV light harvesting features.[36,37] Phenothiazine, on the other hand, has an unconventional puckered structure besides being electron rich in nature.[38-40] Due to its puckered, out-of-plane, butterfly-like structure its self-aggregation in the solid state is hindered, favouring AIE.[41-43]

The work reported here aims to take advantage of the properties of triphenylamine and phenothiazine as OFs for WLE. Herein, two OFs have been designed and synthesised *via* facile reaction to give triphenylamine and phenothiazine based Schiff bases **TPA-SB** and **PTz-SB**, respectively. Both the compounds showed promising AIEE behaviour. Moreover, when these moieties were mixed with rhodamine B dye, desirable WLE was obtained both in solution and gel phases, owing to the phenomenon of FRET. The details of WLE behaviour of the Schiff bases were thoroughly examined by fluorescence titration, spectral overlap studies and fluorescence lifetimes. Furthermore, the AIEE nature of the molecules was investigated through dynamic light scattering (DLS) experiment and TEM studies. Further, DFT and morphological studies were also carried out to examine other interesting aspects of the molecules.

On a parallel note, copper at low concentration plays a crucial role in living organisms in various biological processes.[44-46] Nevertheless, exposure to high concentration of copper is considered potentially toxic and may lead to gastrointestinal disturbances, Alzheimer disease, liver or kidney damage, bipolar disorder, hypothyroidism and Hashimoto's disease.[47-50] The maximum acceptable concentration of copper in drinking water is 2 ppm as recommended by World Health Organization (WHO).[51] Furthermore, the action level of copper is regulated to be 1.3 ppm by the U.S. Environmental Protection Agency (EPA).[52] Several instrumental techniques have been utilized for the quantitation of copper *viz.* atomic absorption spectrometry,[53] inductively coupled plasma mass spectrometry[54] and various electrochemical methods.[55,56] No doubt these techniques have demonstrated good accuracy but the cost and sophistication of these instruments is a big hurdle in their implementation in real life problems on large scale. Hence, there is a high demand of simple yet highly selective and sensitive method for copper detection. Fluorescence methods owing to their easy signal readout, low cost and extreme sensitivity have been widely explored for sensing purpose.[57] Recently, Wu *et al*., reported the synthesis of polyelectrolyte which was utilized to sense Copper at 0.97 ppb level, but the synthesis of the electrolyte was complicated and required multiple steps.[58] With the view to explore the possibility of selective copper sensing and to expand the scope of the easily synthesised Schiff bases, **TPA-SB** and **PTz-SB**, binding studies with Cu (II) were also carried out, the results of which are also presented.

Results and discussions

Synthesis

Both the Schiff bases, **TPA-SB** and **PTz-SB**, were synthesized for the first time using the standard literature procedures. For the synthesis of triphenylamine based Schiff base **TPA-SB**, at first triphenylamine (**1)** was formylated to give triphenylaminealdehyde, **TPA-CHO.** Then, **TPA-CHO** was reacted with tris(2-aminoethyl)amine in methanol at room temperature for 2 hours to give the required moiety **TPA-SB** (Scheme S1, ESI). On the other hand, for the synthesis of phenothiazine based Schiff base **PTz-SB**, first phenothiazine (**2)** was alkylated with hexyl bromide to give hexylphenothiazine (**3)**, which on formylation resulted in the formation of hexylphenothiazinealdehyde, **PTz-CHO**. Then, **PTz-CHO** on reaction with tris(2-aminoethyl)amine in methanol at reflux conditions for 12 h, yielded the desired **PTz-SB** (Scheme S2, ESI). The structures of **TPA-CHO**, **PTz-CHO**, **TPA-SB** and **PTz-SB** were characterized by spectroscopic tools and found to be consistent with that expected (elaborate spectroscopic characterization data of the precursor aldehydes and the Schiff bases are given in the ESI, Fig. S1-S8). The structures of **TPA-SB**, **PTz-SB** and rhodamine B (**Rh-B**) are shown Scheme 1.

Photophysical Studies

The UV-visible and fluorescence spectra of the Schiff bases and their respective precursor aldehydes were recorded in 10^{-5} M DCM solution. The UV-visible and fluorescence spectra of the Schiff bases and the spectra for the respective aldehydes are shown in Fig. S9 and S10 (ESI), respectively. The inset of Figure S9 (ESI) shows the photographs of the Schiff bases under UV light illumination. The absorption spectra of **TPA-SB** and **PTz-SB** showed absorption maxima at 344 nm for both in DCM, which could be attributed to the π-π^* transition. Time dependent DFT studies (TD-DFT) predicts three transitions, which was not observed experimentally, possibly due to the poor resolution of the spectrometer used. As compared to their aldehydes **TPA-CHO** and **PTz-CHO**, there was a blue shift of 9 nm and 35 nm in the λ_{max} for **TPA-SB** and **PTz-SB**, respectively. On the other hand, the emission spectra of **TPA-SB** and **PTz-SB** showed emission maxima at 437 nm and 486 nm, respectively in DCM. Here also, there was a blue shift of 52 nm and 44 nm, in the λ_{max} of **TPA-SB** and **PTz-SB** as compared to that of **TPA-CHO** and **PTz-CHO**, respectively. The blue shift can be attributed to the higher π-π^* band gap for C=N as compared to that for C=O, hence higher energy is required to excite the Schiff bases as compared to their respective aldehydes. The quantum yields for the emission of

View Article Online
DOI: 10.1039/C8NJ03316A

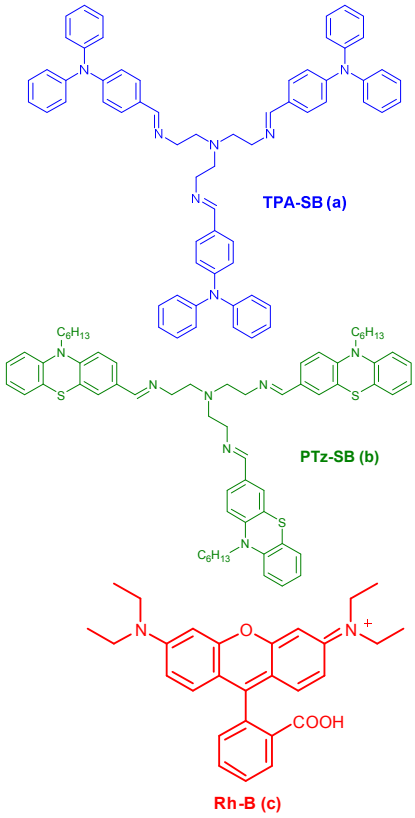

Scheme 1 (a-c) Chemical structures of **TPA-SB**, **PTz-SB** and **Rh-B**

TPA-SB and **PTz-SB** were measured using anthracene and fluorescein, respectively, as standards in THF. The quantum yields for the emission were found to be 0.13 and 0.22 for **TPA-SB** and **PTz-SB**, respectively.

Furthermore, the optical band gaps were calculated for the Schiff bases using the formula $E_g = 1240/\lambda_{onset}$ in 10^{-5} M DCM solution. The E_g values were found to be 2.82 and 2.59 eV for **TPA-SB** and **PTz-SB**, respectively. The values are characteristic for bluish-green and green emission, respectively.

Aggregation-Induced Enhanced Emission (AIEE)

In the case of the Schiff bases **TPA-SB** and **PTz-SB**, aggregation studies were carried out in THF-water mixture with 0 to 90 % water fractions with a constant concentration of 10^{-5} M for each measurement. The absorption and emission spectra of **TPA-SB** are presented in Fig. 1, while that for **PTz-SB** are presented in Fig. S11 (ESI). For **TPA-SB** in THF with 0 % water, the compound showed λ_{max} emission at 466 nm. For 80 % water, there was an 8 fold increase in the fluorescence intensity along with a blue shift of 46 nm in the λ_{max} of emission as compared to that for 0 % water as shown in Fig. 1 (b). The quantum yield value for 80 % water was found to be 0.70, which is significantly higher than that measured for 0 % water (Φ_{PL} = 0.13). In addition to this, in the UV-visible spectrum for the 80 % water fraction, there was tailing-off in the higher wavelength region, which indicates the formation of nano-aggregates [can be inferred from Fig. 1(a)]. Furthermore, there was a colour change from pale green (for 0 % water) to dark blue for 80 % water. But when the water percentage was increased beyond 80 % i.e. for 90 % water, again loss in the fluorescence intensity was observed probably due to the precipitation of the molecules. Similarly, for **PTz-SB**, AIEE property was studied. In fact, in this case for the 90 % water fraction, there was 2.4 fold increase in the fluorescence intensity as compared to that for 0 % water [as shown in ESI Figure S11(b)]. There were two peaks in the emission spectrum in pure THF with λ_{max} of 542 nm and 587 nm. For 90 % water, on the other hand, the higher wavelength peak almost disappeared while the first peak was blue shifted and appeared at a λ_{max} of 520 nm. As in the case of **TPA-SB**, in the case of **PTz-SB** also there was a blue shift of 22 nm in the λ_{max} of emission for 90 % water as compared to that for pure THF. Moreover, tailing-off in the higher wavelength region known as the Mie or light scattering effect was observed in the UV-visible spectra, marking the formation of aggregates as shown in ESI Fig. S11(a).

For high water fraction samples, the formation of aggregates was confirmed by dynamic light scattering experiment (DLS) and TEM studies. The DLS studies revealed that in case of **TPA-SB** for 70 % water, large aggregates of diameter ~ 955 nm were formed, but as the content of water in the solvent mixture was increased further, a decrease in the diameter was observed. For instance, the diameters of the aggregates were 712 and 531 nm for 80 % and 90 % water, respectively. Similar trends were observed for **PTz-SB**, where the diameters of the aggregates were 824, 824 and 458 nm for 70 %, 80% and 90 % water, respectively. The DLS plots are shown in ESI Fig. S12-S13 for **TPA-SB** and **PTz-SB**, respectively. The decrease in the size of the aggregates with the increase in water content for AIE systems is well reported in the literature. The results obtained in this case exactly comply with that.[59-61] Moreover, the aggregation of the particles in the case of **TPA-SB** with increase in water content was further confirmed by TEM studies. The agglomeration of the molecules was observed with the increase in water percentage as shown in Fig. S14 (ESI). Thus, in both the cases, AIEE phenomenon is observed, which might be attributed to the hydrogen bonding taking place between water and the –C=N bond of the Schiff bases. In fact, aggregation was observed only for the higher concentration of water (80 % for **TPA-SB** and 90 % for **PTz-SB**). The AIEE nature is less prominent in case of **PTz-SB** as compared to that in **TPA-SB**. The observation of better AIEE in the case of **TPA-SB** at relatively lower concentration of water could be due to its simpler and relatively better symmetrical structural features that enable better aggregation and therefore more RIM.

It is reported in the literature that in some cases the AIE phenomenon associated with the Schiff bases is mainly due to the hydrolysis of the Schiff base in presence of water to their respective precursor aldehydes.[62] Thus such Schiff bases cannot be termed as AIEgens. In order to investigate, whether the present Schiff bases are really AIEgens, the aggregation properties of **TPA-CHO** and **PTz-CHO** were thoroughly investigated. As already discussed, in case of **TPA-SB**, there

View Article Online
DOI: 10.1039/C8NJ03316A

was a significant blue shift of 46 nm for 80 % water, which resulted in the 8-fold increase in PL intensity. But **TPA-CHO** has emission maximum at 497 nm, which is 33 nm red-shifted than that of **TPA-SB**. This clearly reflects that the AIE profile of **TPA-SB** nowhere matches with the fluorescence profile of **TPA-SB**. Hence **TPA-SB** is infact a AIEgen with significant AIEE properties. For further clarity, the aggregation caused quenching (ACQ) behaviour of **TPA-CHO** is shown in ESI Fig. S15 and S16. This includes the complete absorption and emission profiles for 0 to 90 % water and the DLS studies. Similarly, in case of **PTz-SB** also the emission spectrum for 90 % water does not match with the emission spectra of **PTz-CHO**. The spectral details associated with the ACQ studies of **PTz-CHO** are shown in ESI Fig. S17 and S18. The ACQ nature of both the aldehyde derivatives is evident from the quantum yield measurements. Both the derivatives have comparatively high quantum yields of 37 and 19 % for **PTz-CHO** and **TPA-CHO** in THF solution, respectively. While for 90:10 ratio of water:THF, the quantum yield is less than ~1 %.

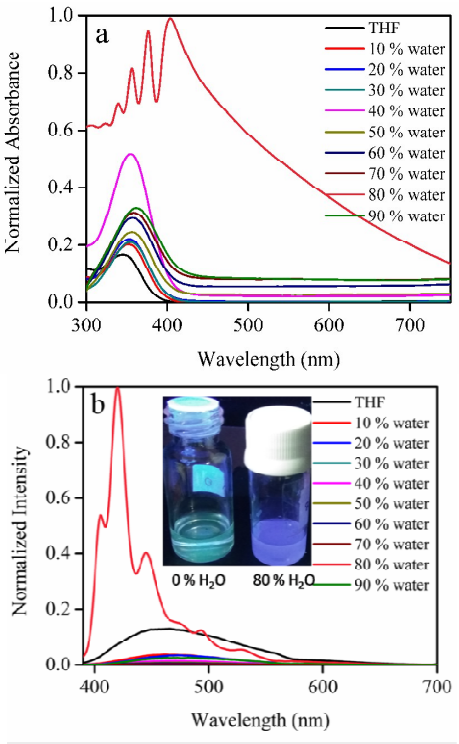

Fig. 1 The absorption (a) and emission (b) spectra of **TPA-SB** in THF-water mixture with different water fractions. Inset in Figure (b) shows the photographs of **TPA-SB** for 0 % water and 80 % water under UV light illumination.

White Light Emission

The emission spectrum of a mixture of 1 mL of **TPA-SB** (in DMF), 1.4 mL of **PTz-SB** (in DMF) and 1 mL of **Rh-B** (in water) each of initial concentration 10^{-5} M is shown in Fig. 2(a). When this solution was excited with UV-light of wavelength 344 nm, white light was emitted with Commission Internationale de L'eclairage (CIE) coordinates of x = 0.32, y = 0.34 [Fig. 2(b)], which were very close to those of the standard CIE for pure white light *viz.* (0.33, 0.33). Furthermore, two fluorescence bands were observed with λ_{max} 490 and 582 nm. The band at 490 nm is due to the combined spectra of the two Schiff bases, while the peak at 582 nm may be attributed to **Rh-B**. The emission spectra for the combination along with the corresponding CIE values are shown in Fig. 2. Moreover, the correlated colour temperature (CCT) of 6115 K was obtained, which reflects that the white light is cool in nature.

In a control experiment, **TPA-SB** and **Rh-B** (1 mL each of initial concentration 10^{-5} M) were mixed. The CIE coordinates for the emission were (0.32, 0.22), which did not correspond to WLE. Similarly, in another control experiment, **PTz-SB** and **Rh-B** were also mixed (initial concentration 10^{-5} M each) and their fluorescence spectrum recorded. But the CIE coordinates (0.37, 0.32) were also not anywhere near to the standard CIE for WLE. The spectra for both combinations are shown in Fig. S19 (ESI). In another control experiment, **TPA-SB** and **PTz-SB** were mixed and fluorescence was recorded. As there was no complementary colour combination possible for this, hence there was no chance of WLE. Conclusively, all the three moieties **TPA-SB**, **PTz-SB** and **Rh-B** are indispensable in the ratio 1:1.4:1 for the generation of white light, as confirmed by the test experiments. The effect of change in concentration of the molecules on white light emission was studied. At first, the concentration of **TPA-SB** and **Rh-B** was kept constant at 1 mL (10^{-5} M each) and the concentration of **PTz-SB** was increased in aliquots of 0.1 mL (10^{-5} M). At 1:1:1 ratio of **TPA-SB: PTz-SB: Rh-B**, the emission intensity due to peak at 582 nm (mainly due to **Rh-B**) was greater than that of the peak around 490 nm

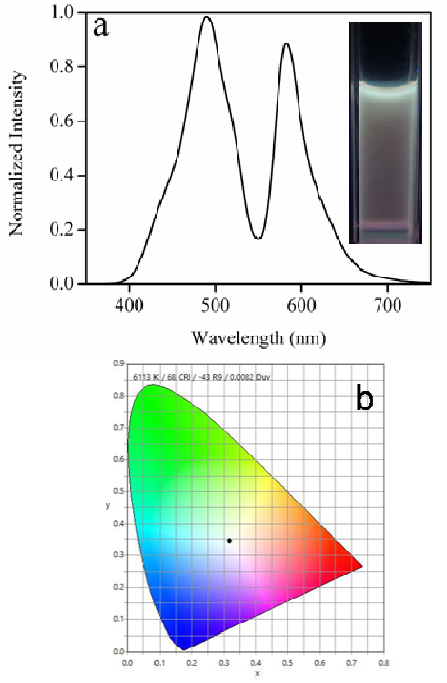

Fig. 2 (a) Emission spectrum of mixture of **TPA-SB** (1. mL 10^{-5} M, in DMF), **PTz-SB** (1.4 mL 10^{-5} M, in DMF) and **Rh-B** (1 mL 10^{-5} M, in water) in solution state, excited at 344 nm. Inset shows the photograph of the corresponding white light under UV light irradiation. (b) CIE diagram of the corresponding white light emission in solution state.

View Article Online
DOI: 10.1039/C8NJ03316A

(due to **TPA-SB** and **PTz-SB**). On further increasing the concentration of **PTz-SB**, at 1:1.4:1, the right intensity match was observed due to the two peaks, which led to the ideal WLE. The CIE chromaticity diagram and the corresponding fluorescence titration spectra are shown in Fig. 3(a) and 3(b), respectively. Hence, 1:1.4:1 molar ratio was the optimized value to obtain pure white light emission. Similarly, the concentration of **TPA-SB** was varied keeping the concentration of **PTz-SB** and **Rh-B** constant, the results of which are shown in ESI Figure S20(a). Then, the concentration of **Rh-B** was varied keeping **TPA-SB** and **PTz-SB** constant [ESI Figure S20 (b)]. These experiments did not give appropriate CIE values required for pure white light emission. Thus, the intensity match of the two peaks is critical for efficient white light emission. The intensity match depends on energy transfer and hence on spectral overlap between the molecules, which eventually leads to efficient white light emission.

In order to further broaden the utility of WLE, the emission was tested in gelatine gel phase. Successfully, three fluorescence bands at 447 nm, 503 nm and 580 nm, with CIE coordinates of (0.31, 0.34) were observed for the ratio 1.4:1.8:1 of **TPA-SB**: **PTz-SB**: **Rh-B**, respectively (Fig. 4). The CCT value obtained was 6500 K, which is a signature of cool white light. Hence, WLE with excellent CIE was obtained in both solution and gel phase. The emission was persistent and robust and moreover, was achieved at room temperature without the application of any harsh conditions. Further, the CCT values obtained in both the cases hint toward cool white light (as it is more than 4500 K).

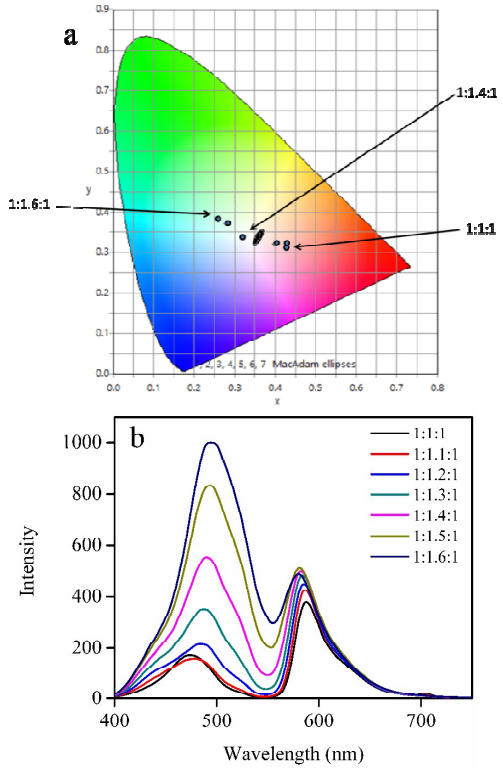

Fig. 3 (a) CIE chromaticity diagram for changing volume of **PTz-SB** from 1 mL to 1.6 mL, keeping volume of **TPA-SB** and **Rh-B** at 1 mL each. (b) The corresponding fluorescence titration spectra.

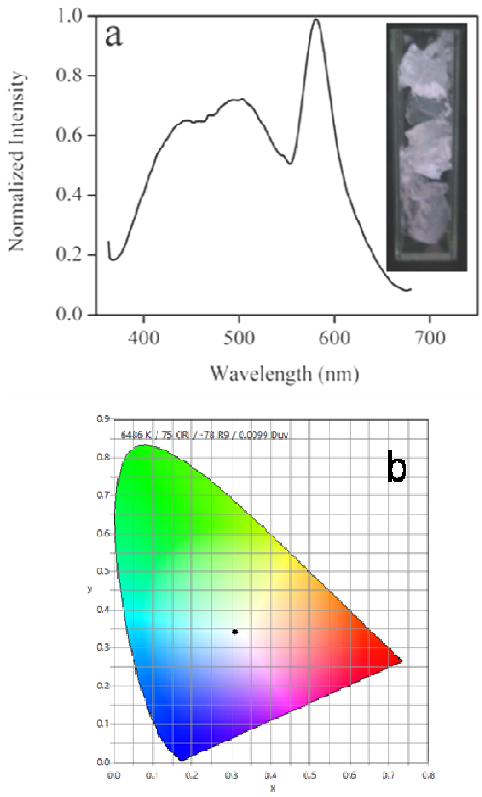

Fig. 4 (a) Emission spectrum of mixture of **TPA-SB** (1.4 mL 10^{-5} M, in DMF), **PTz-SB** (1.8 mL 10^{-5} M, in DMF) and **Rh-B** (1 mL 10^{-5} M, in water) in gelatine gel, excited at 344 nm. Inset shows the photograph of the corresponding white light under UV light irradiation. (b) CIE diagram of the corresponding white light emission in gel phase.

Evaluating the mechanism

The spectral overlap [$J(\lambda)$], energy transfer efficiency (E) and rate of energy transfer (k) were evaluated as reported earlier by us.[63] The possibility of FRET was examined by carrying out spectral overlap study, fluorescence titration and fluorescence lifetime experiments. For the spectral overlap study, the emission spectra of the donors were overlapped with the absorption spectra of the acceptors. Significant overlap was observed between the emission spectrum of **TPA-SB** and the absorption spectrum of **Rh-B.** In fact, the spectral overlap $J(\lambda)$ was found to be 1.40×10^{14} $M^{-1}cm^{-1}nm^4$ for this donor-acceptor pair. The energy transfer efficiency and rate of energy transfer were found to be 69.6 % and 4.19×10^8 s^{-1}, respectively. Similarly, a good spectral overlap between the emission spectrum of **PTz-SB** and the absorption spectrum of **Rh-B** was observed with a spectral overlap $J(\lambda)$ value of 1.15×10^{14} $M^{-1}cm^{-1}nm^4$. Here, the values of E and k were measured to be 17.7 % and 4.54×10^7 s^{-1}, respectively. The values of all the three parameters were good but less than that for the **TPA-SB** and **Rh-B** pair. Nevertheless, the spectral overlap was found to be poor between the emission spectrum of **TPA-SB** and the absorption spectrum of **PTz-SB** with a spectral overlap $J(\lambda)$ value of 9.72×10^{12} $M^{-1}cm^{-1}nm^4$, which was significantly lower than that in the other two cases. The energy transfer

View Article Online
DOI: 10.1039/C8NJ03316A

efficiency and rate of energy transfer were also less significant with the values of 1.09 % and 4.19 × 10^6 s^{-1}, respectively. It can thus be inferred that energy transfer takes place from **PTz-SB** to **Rh-B** and from **TPA-SB** to **Rh-B**, but insignificant energy transfer happened between **TPA-SB** and **PTz-SB**. All the spectral overlap spectra are shown in Fig. S21 (ESI).

Fluorescence titration experiment

The conclusion drawn from spectral overlap studies was supported by the fluorescence titration experiments. In this experiment, the concentration of the donor moiety was kept constant, while the acceptor concentration was increased gradually. If there is a decrease in the fluorescence intensity of the donor with the concomitant increase in the fluorescence intensity of the acceptor, then FRET is operational. Thus, at first, to a solution of **TPA-SB** in DMF (1 mL of 10^{-4} M), **PTz-SB** was added such that concentration of **PTz-SB** gradually increased from 1 µM to 7 µM (for example, first 1 mL each of 10^{-4} M **TPA-SB** was taken in 8 cuvettes; then in the first cuvette 9 mL of DMF was added to give 10^{-5} M solution of **TPA-SB**. Similarly, in the second cuvette, 8 mL of DMF was added along with 1 mL of 10^{-5} M **PTz-SB**, to give 10^{-5} M **TPA-SB** and 1 µM **PTz-SB**. Other solutions were made similarly). The results from these experiments are shown in Fig. 5. As shown in Fig. 5(a), there was no marked decrease in the fluorescence intensity of **TPA-SB** at around 460 nm with the increase in the concentration of **PTz-SB,** although slight red shift and broadening of the peak were observed. Likewise, the titration experiment was repeated for the **PTz-SB** (donor) and **Rh-B** (acceptor). As is evident from the Fig. 5(b), in this case and in contrast to the earlier case, a decrease in the fluorescence intensity of **PTz-SB** was observed at around 488 nm with the concomitant increase in the fluorescence intensity of **Rh-B** at around 582 nm. The titration experiment was repeated for the **TPA-SB** and **Rh-B** pair as shown in Fig. 5(c). Here also a decrease in the fluorescence intensity of the donor (**TPA-SB**) at around 460 nm was observed with the subsequent increase in the fluorescence intensity of the acceptor (**Rh-B**) at around 583 nm.

Fluorescence Lifetime Study

Finally, lifetime experiments were also carried out to confirm FRET. The lifetime spectra for all the three donor-acceptor pairs are shown in Fig. S22 (ESI), also the fluorescence decay parameters of the donors and donors along with the acceptors are shown in ESI Table S1. For this, the lifetimes of the donor and the donor along with the acceptor were recorded. The average lifetime of **TPA-SB** in the excited state was found to be 2.73 ns, while that for **TPA-SB** along with **PTz-SB** was found to be 2.70 ns. Thus, a very minute decrease in the lifetime was observed for this donor-acceptor pair. The average lifetime for **TPA-SB** along with **Rh-B** was recorded then. In this case, there was a sharp decrease in the lifetime from 2.73 ns (for **TPA-SB**) to 0.83 ns for **TPA-SB** along with **Rh-B**. Finally, for the **PTz-SB** and **Rh-B** donor-acceptor pair the lifetimes were recorded. For **PTz-SB** alone the lifetime was found to be 9.71 ns, while that for the mixture of **PTz-SB** and **Rh-B**, the lifetime was found to be 7.94 ns. Clearly, in this case also energy transfer can take place through FRET. As is evident from ESI Table S1, **PTz-SB** showed a two component decay profile. The reason for this may be the existence of two conformation of **PTz-SB** in the excited state. Similarly, when the lifetime of **PTz-SB** was recorded along with **Rh-B**, again biexponential decay was observed. In fact, decrease in both τ_1 and τ_2 was verified for this donor-acceptor pair as compared to pure **PTz-SB**. In contrast, **TPA-SB** showed only one decay component. This is the reason that all the decay profiles, which contains **TPA-SB** as the donor, have single component decay curves. Further, the energy transfer efficiency was also calculated using the lifetime studies by applying the equation:

$$E = 1 - \tau_{DA}/\tau_D \quad (1)$$

where, τ_D is the lifetime of the pure donor, while τ_{DA} is the lifetime of the donor along with the acceptor. The values thus calculated are 1.1 %, 18.2 % and 69.5 % for the pairs **TPA-SB** to **PTz-SB**; **PTz-SB** to **Rh-B** and **TPA-SB** to **Rh-B**, respectively. Thus, from all the three studies it can be concluded that FRET is operational between the respective donor-acceptor pairs. Although the energy transfer from **TPA-SB** to **PTz-SB** is insignificant, yet partial energy transfer cannot be ruled out for this pair. All these observations lead to the conclusion that FRET is responsible for the energy transfer taking place from **TPA-SB** to **PTz-SB** to **Rh-B.** The FRET mechanism is illustrated elaborately in Scheme 2.

DFT Studies

In order to get insight into the electronic distribution of the Schiff bases, gas phase density functional theory (DFT) calculations (B3LYP/6-31G* level) were carried out and compared with that of the precursor aldehydes using Gaussian 09 software.[64-66] It is to be noted that, while carrying out the DFT studies, the $-C_6H_{13}$ chains in **PTz-SB** were replaced by methyl groups in order to reduce the computational cost. The lowest vibrational frequencies (first twenty) for **TPA-SB** and **PTz-SB** are listed in ESI Table S2 and S3, respectively. The computed frequencies are positive in both the cases. The HOMO, H-1, H-2, LUMO, L+1 and L+2 contours were generated for the Schiff bases to get clear insight of the electronic distribution. Similarly, HOMO, LUMO contours were generated for the aldehydes. All the important orbital contours are shown in ESI Fig. S23-S28. In case of the aldehydes (ESI Fig. S23), the HOMO contours are present in the fused aromatic rings i.e. on triphenyl amine and phenothiazine for **TPA-CHO** and **PTz-CHO**, respectively, while the LUMO contours are predominantly present on the aldehyde unit. This is quite obvious, because aldehyde is well known for its electron withdrawing nature. In contrast, in case of the Schiff bases, the HOMO as well as LUMO contours shifts from one aromatic ring to another. However, trace amount of HOMO can be found on

View Article Online
DOI: 10.1039/C8NJ03316A

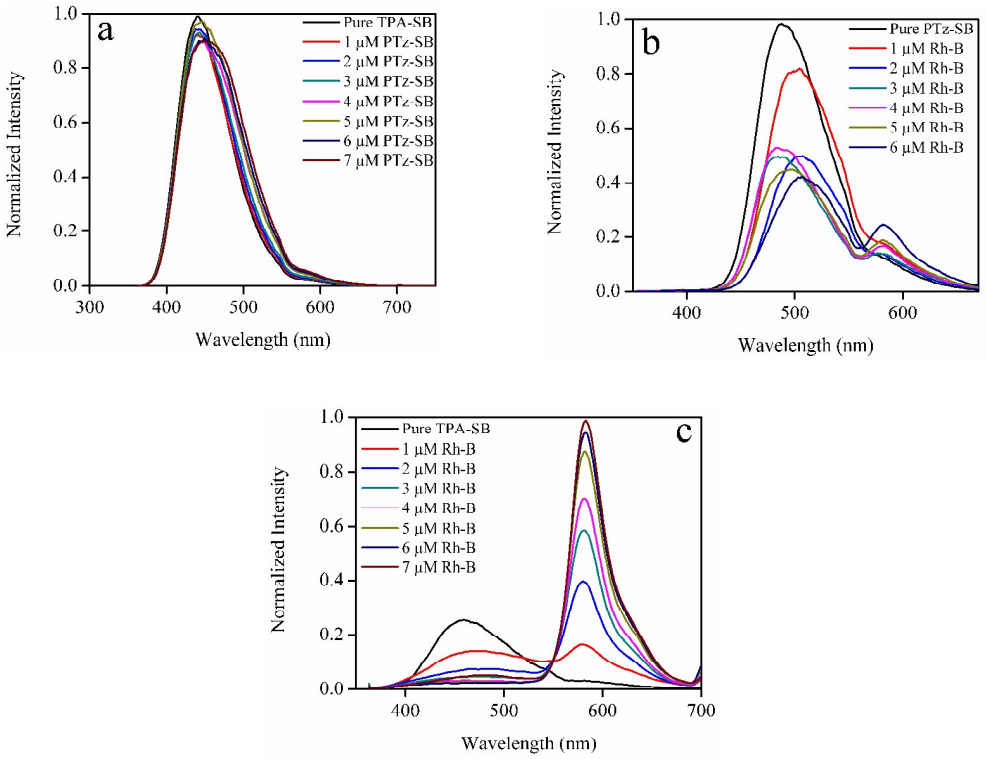

Fig.5 (a) Fluorescence spectrum of **TPA-SB** (10^{-5} M, in DMF) with the addition of **PTz-SB** (in DMF) excited at 344 nm. (b) Fluorescence spectrum of **PTz-SB** (10^{-5} M, in DMF) with the addition of **Rh-B** (in water) excited at 344 nm. (c) Fluorescence spectrum of **TPA-SB** (10^{-5} M, in DMF) with the addition of **Rh-B** (in water) excited at 344 nm.

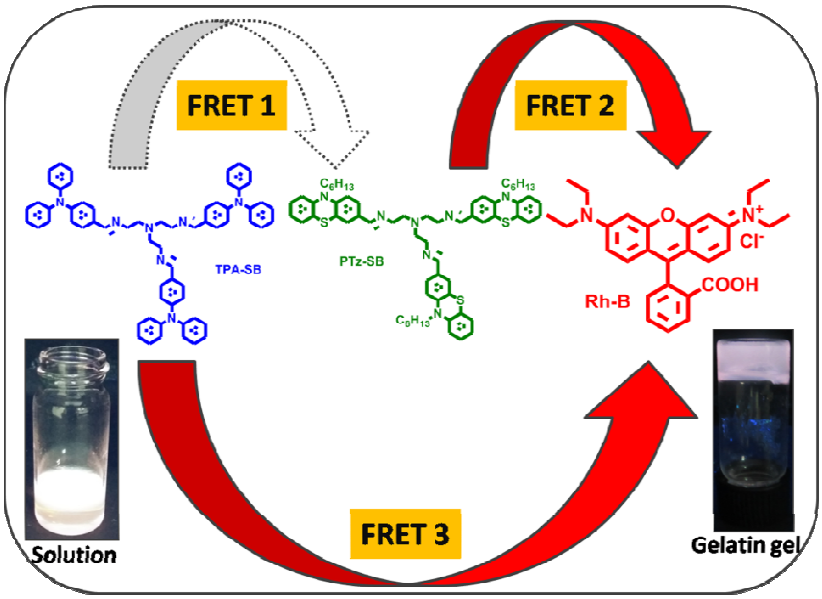

Scheme 2 Schematic presentation of FRET for a mixture of **TPA-SB**, **PTz-SB** and **Rh-B** in solution along with their molecular structures.

View Article Online
DOI: 10.1039/C8NJ03316A

the imino units also. This is because in the Schiff bases no strong electron donor-acceptor moieties are present as N and C have not much electronegativity difference. Hence, all the DFT generated electronic distributions are in accordance with our expectations. Moreover, the presence of HOMO on imino unit is expected due to electron donating nature of nitrogen, which is also reflected from the Cu^{2+} sensing nature of the Schiff bases. Furthermore, in order to compare the experimental UV-visible spectra, time dependent DFT calculation (TD-DFT) was also carried out in DCM solvent (same solvent in which UV-visible spectra were measured) in terms of the three transitions $S_0 \rightarrow S_1$, $S_0 \rightarrow S_2$ and $S_0 \rightarrow S_3$ for both the Schiff bases and compared with the most prominent transitions of the corresponding aldehydes. The electronic transitions, percentage of orbital contributions, the oscillator strength and wavelength are shown in ESI Table S4. The theoretical UV-visible λ_{max} for $S_0 \rightarrow S_1$, transitions are blue-shifted for the Schiff bases as compared to that of their respective aldehydes, which is in accord with the experimental findings. Moreover, three very close transitions are predicted by TD-DFT, which is not observed experimentally, possibly due to the poor resolution of the spectrometer used. Further, in order to find out the effect of change in dihedral angle (ϕ) on the energy of **TPA-SB**, a graph of ΔE *vs.* ϕ was plotted. For this, the dihedral angle chosen was between the central nitrogen and the nitrogen atom of one of the –C=N units (the specific four atoms chosen for the calculations are shown by black spots and numbered 1-4 in the inset structure of **TPA-SB** of ESI Fig. S29); the angle was changed from 180 to 110°. It could be inferred (ESI Fig. S29) that when the dihedral angle was decreased beyond 125°, there was a sudden incremental jump in the energy of the molecule. Thus, freezing of the segmental motion is necessary for the stabilization of the molecule, which may lead to AIEE behaviour. Thus, overall the DFT studies are in good agreement with the experimental findings.

Morphology

In order to study the morphology of the Schiff bases, high resolution scanning electron microscopy (HR-SEM) and transmission electron microscopy (TEM) were employed. The SEM images of the Schiff bases for **TPA-SB** and **PTz-SB** are shown in Fig. 6(a) and 6(b), respectively, while TEM image for **TPA-SB** is shown in Fig. 6(c). These revealed the formation of spherical morphology for **TPA-SB** in THF solution consistent with its relatively simpler and more symmetrical structure. In fact, the average size of the particles was in the range of 500-600 nm as verified by the particle size analysis [inset Figure 6(c)]. **PTz-SB** on the other hand, showed nano-sized pyramidal shape. This pyramidal morphology may be due to the relatively lesser symmetry arising out of the butterfly-like structure of phenothiazine backbone that is complicated further by the presence of long alkyl side chains attached to the phenothiazine. The average size of the particles in this case was in the range 80-90 nm. These AIEE spheres and nanopyramids can have promising utilities in the fields of fluorescence imaging, biological cell tracing and heavy metal sensing.

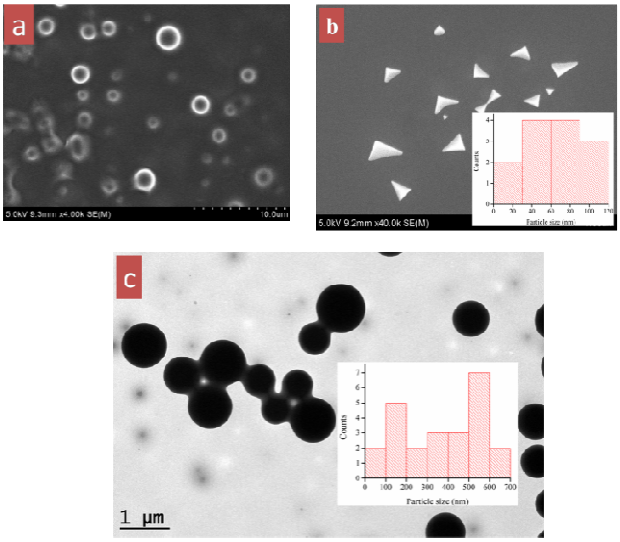

Fig. 6 (a) SEM images of **TPA-SB** in THF, scale is 10.0 μm. (b) SEM images of **PTz-SB**, scale is 1.0 μm. (c) HR-TEM image of **TPA-SB** in THF. Inset shows the particle size distribution analysis.

TGA and DSC studies

The thermal properties of the compounds **TPA-SB** and **PTz-SB** were determined by thermogravimetric analysis (TGA) and differential scanning calorimetry (DSC) analysis, which were carried out under N_2 atmosphere at a heating rate of 5 °C/min. Both the Schiff bases showed extremely high thermal stability with the decomposition temperatures of 308 and 312 °C at 5 % weight loss for **TPA-SB** and **PTz-SB**, respectively. Moreover, the DSC studies revealed the melting temperatures of 137 °C and 101 °C for **TPA-SB** and **PTz-SB**, respectively. Such high decomposition and melting temperatures of the Schiff bases are due to the presence of fused aromatic systems. Such high thermal robustness is essential in optoelectronics from device fabrication point of view. The TGA and DSC of the compounds are shown in ESI Fig. S30-S31.

Copper (II) sensing and selectivity studies

Schiff bases are well known to form stable complexes with Cu(II) ion. The binding of **TPA-SB** towards Cu^{2+} cation and its consequence on its fluorescence was verified through fluorescence titration experiments as shown in Fig. 7. As is evident from the Fig. 7(a), there was a continuous decrease in the fluorescence intensity of **TPA-SB** (10^{-5} M in DMF) on sequential addition of copper ion in water (0.5 ppb to 10 ppb). Along with the decrease, a red-shift in the λ_{max} of emission was also observed from 441 nm (0 ppb) to 469 nm (10 ppb). In order to quantify the quenching efficiency, the fluorescence intensity of **TPA-SB** was plotted against [Cu^{2+}] ions (Stern-Volmer plot as per equation 3) as shown in Fig. 7(b).

View Article Online
DOI: 10.1039/C8NJ03316A

$$I_0/I = 1 + K_{SV}[Cu^{2+}] \quad (2)$$

Here I_0 and I are the fluorescence intensity of **TPA-SB** in the absence and presence of Cu^{2+} ion, respectively. K_{SV} is the Stern-Volmer constant and $[Cu^{2+}]$ is the concentration of Cu^{2+} ions. This plot was used to calculate the limit of detection (LOD) using the equation: LOD = 3σ/s, where σ is the standard deviation of the blank sample and s is the slope of the calibration curve. The LOD was found to be 1.8 ppb. Furthermore, modified Stern-Volmer plot (ESI Fig. S32) was used to calculate the binding constant. The equation used is:[67]

$$\log(I_0/I - 1) = \log K_a + n\log[Q] \quad (3)$$

where, K_a and n are the binding constant and number of binding sites, respectively. K_a value determined from the intercept of ESI Fig. S32 is 9.77×10^{11} M^{-1}. This represents a very strong binding affinity of the Cu^{2+} ions with the Schiff base. Moreover, the binding mode of Cu^{2+} and **TPA-SB** was analysed by fluorescence Job's plot (ESI Fig. S33). For which, the mole ratio of Cu^{2+} was varied and the respective PL intensities were recorded. Minimum intensity was observed for 0.3 mole fraction of Cu^{2+}, indicating the stoichiometry of 1:2 for Cu^{2+}:**TPA-SB**. The quenching mechanism was studied by temperature dependent fluorescence experiment (ESI Fig. S34). For this, to a 10^{-5} M solution of **TPA-SB** in DMF, 1 ppb of Cu^{2+} was added. Then, the temperature was varied from 0 °C to 60 °C. Clearly, there is increased quenching efficiency at higher temperatures, this may be due to larger diffusion coefficients at higher temperature. Hence the quenching observed in this case is dynamic in nature.

In order to investigate if the sensing of Cu^{2+} ions was selective, eleven representative metal cations viz. Cr^{3+}, Cd^{2+}, Cu^{2+}, Fe^{2+}, Hg^{2+}, Ni^{2+}, Sn^{2+}, Zn^{2+}, Co^{2+}, Fe^{3+} and Mn^{2+} were screened. For this purpose, the concentration of the metal ions was 5×10^{-7} M in water, while the concentration of **TPA-SB** was 5×10^{-5} M. The results from the PL studies are shown in Fig. 8(a). As may be observed, only 8 % of the initial intensity of **TPA-SB** remained when copper ion was added. Furthermore, the plot of intensity change (I_0/I) at the emission maximum for the different metal cations is shown in Fig. 8(b). The intensity change (I_0/I) for Cu^{2+} was 12 fold, whereas that for the second most responsive cation i.e. Fe^{3+} was only 1.7 fold. This plot reveals the dramatic selectivity of **TPA-SB** for Cu^{2+} ions as compared to other heavy metal cations.

Since, **PTz-SB** has similar structural attributes (except the fused aromatic ring). Therefore, the Cu^{2+} quenching studies were extended to the **PTz-SB** Schiff base under identical conditions. In this case also, quenching behaviour was observed with a LOD of 4.88 ppb (ESI Fig. S35a). Furthermore, screening of ten representative elements was also studied (ESI Fig. S35b). This Schiff base is also highly selective to Cu^{2+} ions, in presence of the other important cations. In fact, the intensity change (I_0/I) for Cu^{2+} was 13 fold. This study puts light on the mechanism of quenching. It is the N atom of C=N, which is the common attribute in both the Schiff bases, that is leading to the quenching behaviour. In fact, Schiff bases are well known to form strong bond with Cu^{2+} ions.

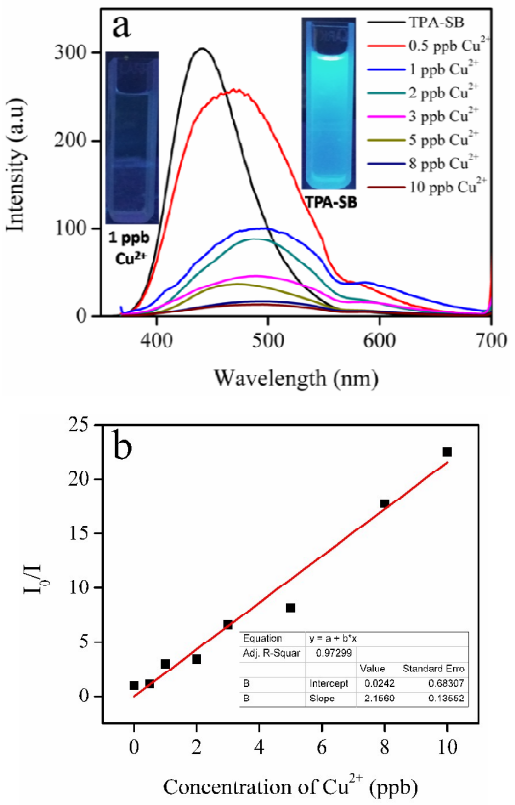

Fig. 7 (a) Emission spectra of **TPA-SB** (10^{-5} M in DMF) with the addition of different concentrations of Cu^{2+}. The inset shows the photographs of **TPA-SB** in absence and presence of 1 ppb of Cu^{2+} ion under UV light. (b) Stern-Volmer plot of **TPA-SB** in presence of different concentrations of Cu^{2+} ion (λ_{exc} = 344 nm)

View Article Online
DOI: 10.1039/C8NJ03316A

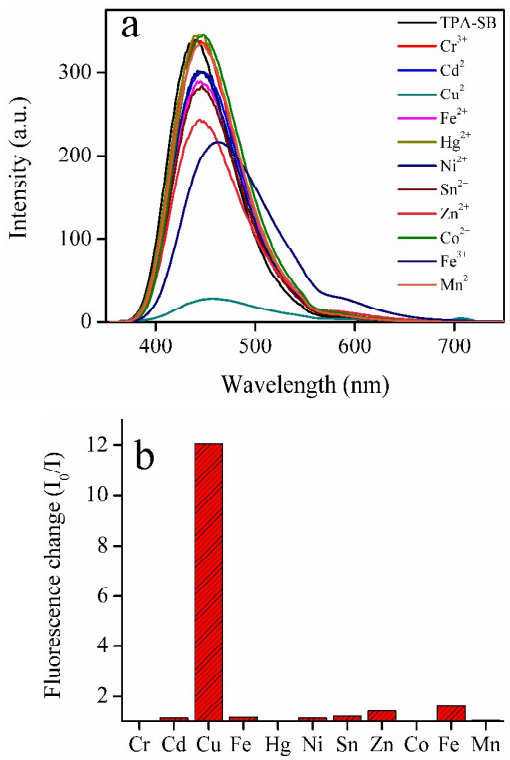

Fig. 8 (a) Emission spectra of **TPA-SB** (5×10^{-5} M in DMF) in presence of different cations (5×10^{-7} M in water). (b) The fluorescence quenching efficiencies (I_0/I) of **TPA-SB** in presence of different cations added separately.

Conclusions

Two new Schiff bases, one triphenylamine (**TPA-SB**) based and another phenothiazine (**PTz-SB**) based were synthesized by simple organic transformations. Both the Schiff bases showed promising aggregation-induced enhanced emission (AIEE) behaviour. In the case of **TPA-SB**, the AIEE phenomenon resulted in an 8-fold increase in fluorescence intensity in an 80:20 THF/water mixture in comparison to pure THF. This increase is attributed to its simpler structure that enables facile aggregation and therefore more restricted intramolecular motions. Furthermore, when these two moieties were mixed with rhodamine dye (**Rh-B**) and photoexcited at 344 nm, efficient white light emission (WLE) was obtained with Commission Internationale d'Eclairage (CIE) coordinates (0.32, 0.34) and (0.31, 0.34) in solution and gelatine gel phase, respectively. Moreover, the correlated colour temperatures obtained in the two phases (6115 K in solution and 6500 K in gelatine gel) suggests that the system emits cool white light. The plausible mechanism behind WLE was Förster resonance energy transfer, which was verified through fluorescence titration experiments, lifetime and spectral overlap studies. The optical band gaps calculated using UV-visble spectroscopy are 2.82 and 2.59 eV for **TPA-SB** and **PTz-SB**, respectively. Furthermore, DFT and morphology studies were also conducted to verify the possibility of using these compounds in optoelectronic applications. Excellent thermal stability was observed for the Schiff bases as confirmed by the TGA and DSC studies. Finally, the emission spectrum of **TPA-SB** showed very high sensitivity and selectivity towards Cu^{2+} in presence of ten other cations. The limit of detection obtained was 1.8 ppb which is way below the EPA action level of 1.3 ppm.

Experimental Section

Chemicals

The compounds tris(2-aminoethyl)amine and phenothiazine were purchased from Sigma Aldrich. Triphenylamine was purchased from Alfa Aesar. All these chemicals were used as such without further purification. The solvents: DMSO, DMF and methanol were purchased from Rankem & Co. and were distilled when necessary, using the standard procedure. The deuterated solvents were purchased from Sigma Aldrich. Gelatin was purchased from S. D. fine-Chem. Pvt. Ltd.

Synthesis of TPA-CHO

To a solution of phosphourous chloride (1.85 mL, 20 mmol) in DMF (5.6 mL) at 0 °C, triphenyl amine (5 g, 20 mmol) was added. The mixture was stirred at 70 °C for 24 h. The mixture was then poured into ice cold water, neutralized with saturated Na_2CO_3 (20 mL). The aqueous layer was extracted with CH_2Cl_2 (3×20 mL). The organic layer was dried over anhydrous sodium sulphate, filtered and concentrated under reduced pressure. Finally the crude product was purified by silica gel chromatography to give light yellow solid. Yield: 85 %, yellow solid. ^{1}H NMR (400 MHz, $CDCl_3$): δ 9.72 (s, 1H), 7.58-7.60 (d, J = 8.50 Hz, 2H), 7.24-7.28 (m, 4H), 7.08-7.10 (m, 6H), 6.92-6.95 (d, J = 8.50 Hz, 2H). ^{13}C NMR (100 MHz, $CDCl_3$): δ 190.62, 153.51, 146.29, 131.47, 129.89, 126.47, 125.27, 119.48. IR (KBr): 2739.72, 1684.21, 1580.57, 1562.883, 1326.31, 1216.10, 973.04, 8821.41, 694.67 cm^{-1}. UV-vis (DCM) λ_{max}: 353 nm. MS (EI) m/z: 274.12 (100 M^+). All the spectral data with assignments are given in ESI Figure S1-S2.

Synthesis of PTz-CHO

To a solution of phosphourous chloride (3.3 mL, 35.9 mmol) in DMF (2.8 mL) at 0 °C, PTz-C_6H_{13} (3.3 g, 9 mmol) was added. The mixture was stirred at 70 °C for 24 h. The mixture was then poured into ice cold water, neutralized with saturated Na_2CO_3 (20 mL). The aqueous layer was extracted with CH_2Cl_2 (3×20 mL). The organic layer was dried over anhydrous sodium sulphate, filtered and concentrated under reduced pressure. Finally the crude product was purified by silica gel chromatography to give light yellow solid. Yield: 80 %, yellow solid. ^{1}H NMR (400 MHz, $CDCl_3$): δ 9.77 (s, 1H), 7.60-7.62 (d, J = 8.50 Hz, 2H), 6.94-7.15 (m, 3H), 6.85-6.87 (d, J = 8.50 Hz, 2H), 3.84-3.87 (t, J = 7.13 Hz, 2H), 1.77-1.81 (m, 2H), 1.41-1.44 (m, 2H), 1.29-1.31 (m, 4H), 0.85-0.888 (m, 3H). ^{13}C NMR (100 MHz, $CDCl_3$): δ 190.12, 150.81, 143.48, 131.07, 130.21, 128.42,

View Article Online
DOI: 10.1039/C8NJ03316A

127.65, 127.65, 127.62, 123.65, 116.04, 114.86, 48.09, 31.47, 26.79, 26.60, 22.67, 14.09. IR (KBr): 2951.65, 2921.50, 1679.888, 1463.55, 1362.43, 1242.14, 1194.94, 862.44, 745.18 cm^{-1}. UV-vis (DCM) λ_{max}: 379 nm. MS (EI) *m/z*: 312.14 (100 M^+). All the spectral data with assignments are given in ESI Figure S3-S4.

Synthesis of TPA-SB

A solution of triphenylamine-1-carboxaldehyde (3 mmol) in methanol (30 mL) was added to a solution of tris(2-aminoethyl)amine (1 mmol) in methanol (10 mL), which resulted in the formation of a yellow precipitate. The reaction was continued for 2 h with stirring at room temperature. Finally, the crude product was washed with cold methanol and dried to give **TPA-SB**. Yield: 65 %, yellow solid. Mp. 137 °C. ^{1}H NMR (400 MHz, $CDCl_3$): δ 8.02 (s, 3H), 7.35-7.37 (d, *J* = 8.64 Hz, 6H), 7.19-7.23 (m, 12H), 7.03-7.07 (m, 18H), 6.97-6.99 (d, *J* = 8.64 Hz, 6H), 3.63-3.65 (t, *J* = 6.0 Hz, 6H), 2.87-2.90 (t, *J* = 6.0 Hz, 6H). ^{13}C NMR (100 MHz, $CDCl_3$): δ 161.33, 149.89, 147.05, 129.35, 129.05, 125.13, 123.63, 121.74, 59.91, 55.84. IR (KBr): 3436, 2200, 1636, 1579, 1490, 1412, 1266, 754, 692 cm^{-1}. UV-vis (DCM) λ_{max}: 344 nm. MS (EI) *m/z*: 912.47 (100 M^+). All the spectral data with assignments are given in ESI Figure S5-S6.

Synthesis of PTz-SB

A solution of phenothiazine-1-carboxaldehyde (3 mmol) in methanol (30 mL) was added to a solution of tris(2-aminoethyl)amine (1 mmol) in methanol (10 mL), which resulted in the formation of an orange precipitate. The reaction mixture was refluxed at 50 °C for 12 h with continuous stirring. Finally, the crude product was washed with cold methanol and dried to give **PTz-SB**. Yield: 60 %, orange solid. Mp. 101 °C. ^{1}H NMR (400 MHz, $CDCl_3$): δ 7.87 (s, 3H), 7.23 (s, 3H), 7.14-7.17 (m, 6H), 7.05-7.07 (m, 3H), 6.83-6.90 (m, 3H), 6.68-6.70 (d, *J* = 8.64 Hz, 6H) 3.78-3.82 (t, *J* = 6.0 Hz, 6H), 3.58 (s, 6H)2.84 (s, 6H), 1.75-1.77 (m, 9H), 1.26-1.40 (m, 15H), 0.84 (s, 9H). ^{13}C NMR (100 MHz, $CDCl_3$): δ 160.58, 146.99, 144.39, 130.56, 127.47, 127.37, 127.12, 126.54, 124.78, 124.32, 122.57, 115.40, 114.92, 59.83, 55.77, 47.63, 31.38, 26.74, 26.56, 22.53, 13.94. IR (KBr): 3447, 2919, 2852, 1639, 1571, 1413, 1015, 1015, 807, 739 cm^{-1}. UV-vis (DCM) λ_{max}: 344 nm. MS (EI) *m/z*: 1026.53 (100 M^+). All the spectral data with assignments are given in ESI Figure S7-S8.

Preparation of White Light Emitting Gelatin Gel

Gelatin gel was prepared by dissolving 0.5 g of gelatine in 10 mL of distilled water (5 % w/v). To this viscous solution, the mixture of 1.4 mL of **TPA-SB** in DMF, 1.8 mL of **PTz-SB** in DMF and 1 mL of **Rh-B** in water (each of initial concentration 10^{-5} M) was added. The final mixture was heated to 65 °C and then placed in the refrigerator, maintained at a temperature of 10 °C, overnight, to obtain the required white gel.

Characterization

Melting points were determined using SUNBIM (India) melting point apparatus. ^{1}H NMR spectra were measured on a BRUKER AVANCE 400 (400 MHz for ^{1}H) spectrometer. The chemical shift values of ^{1}H NMR are expressed in parts per million downfield relative to the internal standard, tetramethylsilane (δ = 0 ppm) or chloroform (δ = 7.26 ppm). Splitting patterns are indicated as s, singlet; d, doublet; t, triplet; q, quartet; m, multiplet. ^{13}C NMR spectra were measured on a BRUKER AVANCE 400 (100 MHz for ^{13}C) spectrometer with tetramethylsilane (δ = 0 ppm) or chloroform-*d* (δ = 77.0 ppm) as internal standard. Chemical shift values are given in parts per million (ppm) downfield relative to the internal standard. Mass spectra were recorded using a Micromass Q-TOF mass spectrometer. Thermogravimetric analysis was performed with TA INSTRUMENTS Q-500 Hi-Res-TGA. UV-visible absorption spectra were recorded on JASCO V-630 spectrophotometer. Fluorescence spectra were measured on FLUOROMAX 4 (Horiba JobinYvon). Fourier transform infrared spectra (FTIR) were recorded on a JASCO FTIR–4500 spectrometer. The SEM images were recorded using a FEG Quanta 400 scanning electron microscope (electron acceleration voltage was 3 kV). The TEM images were recorded using a Philips CM12 transmission electron microscope (electron acceleration voltage was 120 kV). DLS experiments were carried out with ZETASIZER NANO ZS90 MALVERN Instrument.

Acknowledgements

This work was supported by the Indian Institute of Technology Madras (IITM), Chennai, India. Timely help from Suraj Kumar Panigrahi in lifetime studies, Elumalai Ramachandran and Sudip Mandal in DFT studies is heartily acknowledged.

References

1 N. K.Al-Rasbi, H. Adams and F. O. Suliman, *Dyes Pigm*., 2014, **104**, 83-88.
2 A. A.Bahri, A. S.A-Zakwani, S. M. A-Farsi, and N. K. Al-Rasbi, *ChemsitrySelect*, 2016, **1**, 1393-1399.
3 M. C. Gather, A. Kohnen and K. Meerholtz, *Adv. Mater*., 2011, **23**, 233-248.
4 M. Chen, Y. Zhao, L. Yan, S. Yang, Y. Zhu, I. Murtaza, G. He, H. Meng, W. Huang, *Angew. Chem. Int. Ed.,* 2016, **55**, 1-7.
5 S. Mukherjee and P. Thilagar, *Dyes Pigm.,* 2014, **110**, 2-27.
6 B. D'Andrade and S. R. Forrest, *Adv. Mater.,* 2004, **16**, 1585-1595.
7 S. Reineke, *Rev. Mod. Phys.,* 2013, **85**, 1245-1293.
8 H. Wang, Q. Dong, J. Li, X. Fang, Y. Hao, H. Xu, B. Xu and W. Y. Wong, *J. Inorg. Organomet. Polym.,* 2014, **24**, 201-207.
9 P. Malakar, P. Modak, E. Prasad, *Chem. Commun.,* 2016, **52**, 4309-4312.
10 J. Liu, *Spectrochim. Acta, Part A,*2015, **149**, 48-53.
11 M. Kasha, *Discuss. Faraday Soc.,*1950, **9,** 14-19.
12 B. Zhang, L. Liu and Z. Xie, *Isr. J. Chem*., 2013, **53**, 897-917.
13 J. Zhao, S. Ji, Y. Chen, P. Guo and P. Yang,*Phys. Chem. Chem. Phys*., 2012, **14**, 8803-8817.

View Article Online
DOI: 10.1039/C8NJ03316A

14 S. Achelle, J. R. Lopez, C. Katan and F. R. Guen, *J. Phys. Chem. C,* 2016, **120**, 26986-26995.
15 R. Chakrabarty, P. S. Mukherjee and P. J. Stang, *Chem. Rev*., 2011, **111**, 6810-6918.
16 W. –C. Geng, Y. –C. Liu, Y. -Y. Wang, Z. Xu, Z. Zheng, C. –B. Yang and D. –S. Guo, *Chem. Commun*., 2017, **53**, 392-395.
17 Y. -T. Lee, Y. -T. Chang, C. -T Chen, and C. -T Chen, *J. Mater. Chem. C,* 2016 **4**, 7020-7025.
18 S. Samanta, U. Manna and G. Das, *New J. Chem.,* 2017, **41**, 1064-1072.
19 P. Bairi, B. Roy, P. Chakraborty and A. K. Nandi, *ACS Appl. Mater. Interfaces,* 2013, **5**, 5478-5485.
20 T. Pullerits and V. Sundstrom, *Acc. Chem. Res.,* 1966, **29**, 381-389.
21 K. V. Rao, K. K. Datta, M. Eswaramoorthy and S. J. George, *Chem. Eur. J*., 2012, **18**, 2184-2194.
22 V. Singh, A. K. Mishra, *Sci. Rep*., 2015, **5**, 11118.
23 D. K. Maiti, R. Bhattacharjee, A. Datta and A. Banerjee, *J. Phys. Chem. C,* 2013, **117**, 23178-23189.
24 M. T.Bernius, M. Inbasekaran, J. O'Brien and W. Wu, *Adv. Mater*., 2000, **12**, 1737-1750.
25 G. Zhang, J. Sun, P. Xue, Z. Zhang, P. Gong, J. Peng and R. Lu, *J. Mater. Chem. C,* 2015, **3**, 2925-2932.
26 N. Meher and P. K. Iyer, *Angew. Chem. Int. Ed.* 2018, **57**, 1-6.
27 Y. Hong, J. W. Y. Lam and B. Z. Tang, *Chem. Commun*., 2009, 4332-4353.
28 A. Qin, J. W. Y. Lam and B. Z. Tang, *Prog. Polym. Sci*., 2012, **37**, 182-209.
29 S. Chen, Z. Qin, T. Liu, X. Wu, Y. Li, H. Liu, Y. Song and Y. Li, *Phys. Chem. Chem. Phys*., 2013, **15**, 12660-12666.
30 V. Srinivasan, M. A. Jhonsi, N. Dhenadhayalan, K. C. Lin, M. Jaccob and A. Kathiravan, *ChemistrySelect,* 2017, **2,** 1353-1359.
31 M. Sailer, A. W. Franz and T. J. J. Miiler, *Chem. Eur. J.,* 2008, **14**, 2602-2614.
32 J. Cremer and C. A. Briehn, *Chem. Mater.,* 2007, **19**, 4155-4165.
33 M. Yang, D. Xu, W. Xi, L. Wang, J. Zheng, J. Zheng, J. Huang, J. Zhang, H. Zhou, J. Wu and Y. Tian, *J. Org. Chem.,* 2013, **78**, 10344-10359.
34 W. Li, X. Tian B. Huang, H. Li, X. Zhao, S. Gao, J. Zheng, X. Zhang, H. Zhou, Y. Tian and J. Wu, *Biosens. Bioelectron*., 2016, **77**, 530-536.
35 P. S. Hariharan, N. Hari and S. P. Anthony,*Inorg. Chem. Commun*., 2014, **48**, 1-4.
36 Z. Wan, C. Jia, Y. Duan, L. Zhou, Y. Lin and Y. Shi, *J. Mater. Chem*., 2012, **22**, 25140-25147.
37 M. Chen, H. Nie, B. Song, L. Li, J. Z. Sun, A. Qin and B. Z. Tang, *J. Mater. Chem. C,* 2016, **4**, 2901-2908.
38 Y. Hua, S. Chang, D. Huang, X. Zhou, X. Zhu, J. Zhao, T. Chen, W. Y. Wong and W. K. Wong, *Chem. Mater*., 2013, **25**, 2146-2153.
39 M. J. Park, J. Lee, J. H. Park, S. K. Lee, J. I. Lee, H. Y. Chu, D. H. H. Wang and H. K. Shim, *Macromolecules,* 2008, **41**, 3063-3070.
40 P. Xue, B. Yao, J. Sun, Q. Xu, P. Chen, Z. Zhang and R. Lu, *J. Mater. Chem. C,* 2014, **2,** 3942-3950.
41 A. Zabulica, M. Balan, D. Belei, M. Sava, B. C. Simionescu and L. Marin, *Dyes. Pigm*., 2013, **96**, 686-698.
42 K. M. Venganian, C. D. Britto, K. Sekar, G. Sivaraman and S. Singaravadivel, *Sens. Actuator B-Chem.,* 2016, **235**, 232-240.
43 R. K. Konidena, K. R. Thomas, S. Kumar, Y. C. Wang, C. J. Li and J. H. Jou, *J. Org. Chem.,* 2015, **80**, 5812-5823.
44 E. L. Que, D. W. Domaille and C. J. Chang, *Chem. Rev.,* 2008, **108**, 1517-1549.
45 S. S. Leal, H. M. Botelho and C. M. Gomes, *Coord. Chem. Rev.,* 2012, **256**, 2253-2270.
46 H. Q. Lu, D. Samanta, L. S. Xiang, H. M. Zhang, H. X. Hu, I. Chen, J. W. Bullen and G. L. Semenxa, *Proc. Natl. Acad. Sci. U.S.A.,* 2015, **112**, E4600-E4609.
47 R. H. Lei, B. H. Yang, C. Q. Wu, M. Y. Liao, R. G. Ding and Q. J. Wang, *Toxicol. Res.*, 2015, **4**, 351-364.
48 F. Pizarro, M. Olivares, R. Vauy, P. Contreras, A. Rebelo and V. Gidi, *Environ. Health Perspect.,* 1999, **107**, 117-121.
49 E. S. Ford, *Am. J. Epidemiol.,* 2000, **151**, 1182-1188.
50 O. Bandmann, K. H. Weiss and G. G. Kaler, *Lancet Neurol.,* 2015, **14**, 103-113.
51 R. Uauy, A. Maass and M. Araya, *Am. J. Clin. Nutr.,* 2008, **88**, 867S-871S.
52 H. S. Jung, P. S. Kwon, J. W. Lee, J. I. Kim, C. S. Hong, J. W. Kim, S. Yan, J. Y. Lee, J. H. Lee, T. Joo and J. S. Kim, *J. Am. Chem. Soc.,* 2009, **131**, 2008-2012.
53 O. A. Urucu and A. Aydin, *Anal. Lett.,* 2015, **48**, 1767-1776.
54 T. Silberstein, M. Saphier, Y. Mashiach, O. Paz-Tal and O. Saphier, *J. Matern.-FetalNeonat. Med.,* 2015, **28**, 88-92.
55 T. Attar, Y. Harek and L. L. Larabi, *Med. J. Chem.,* 2014, **2**, 691-700.
56 E. S. Almeida, E. M. Richter and R. A. A. Munoz, *Anal. Chim. Acta,* 2014, **837**, 38-43.
57 A. A. Dar, A. K. Dwivedi, P. K. Iyer and A. T. Khan, *Asian J. Green Chem.,* 2018, **2**, 171-180.
58 W. Wu, A. Chen, L. Tong, Z. Qing, K. P. Langone, W. E. Bernier and W. E. Jones, *ACS Sens.,* 2017, **2**, 1337-1344.
59 W. B.Jia, H. W. Wang, L. M. Yang, H. B. Lu, L. Kong, Y. P. Tian, X. T. Tao and J. X. Yang, *J. Mater. Chem. C,* 2013, **1**, 7092-7101.
60 L. Wang, Z. Zheng, Z. Yu, J. Zheng, M. Fang, J. Wu, Y. Tian and H. Zhou, *J. Mater. Chem. C,* 2013, **1**, 6952-6959.
61 L. Wang, Y. Shen, Q. Zhu, W. Xu, M. Yang, H. Zhou, J. Wu and Y. Tian, *J. Phys. Chem C,* 2014, **118**, 8531-8540.
62 B. Pramanik and D. Das, *J. Phys. Chem. C*, 2018, **122**, 3655-3661.
63 V. Anand and R. Dhamodharan, *New J. Chem.,* 2017, **41**, 9741-9751.
64 M. J. Frisch, G. W. Trucks, H. B. Schlegel, G. E. Scuseria, M. A. Robb, J. R. Cheeseman, G. Scalmani, V. Barone, B. Mennucci, G. A. Petersson, H. Nakatsuji, M. Caricato, X. Li, H. P. Hratchian, A. F. Izmaylov, J. Bloino, G. Zheng, J. L. Sonnenberg, M. Hada, M. Ehara, K. Toyota, R. Fukuda, J. Hasegawa, M. Ishida, T. Nakajima, Y. Honda, O. Kitao, H. Nakai, T. Vreven, J. A. Montgomery, Jr., J. E. Peralta, F. Ogliaro, M. Bearpark, J. J. Heyd, E. Brothers, K. N. Kudin, V. N. Staroverov, R. Kobayashi, J. Normand, K. Raghavachari, A. Rendell, J. C. Burant, S. S. Iyengar, J. Tomasi, M. Cossi, N. Rega, J. M. Millam, M. Klene, J. E. Knox, J. B. Cross, V. Bakken, C. Adamo, J. Jaramillo, R. Gomperts, R. E. Stratmann, O. Yazyev, A. J. Austin, R. Cammi, C. Pomelli, J. W. Ochterski, R. L. Martin, K. Morokuma, V. G. Zakrzewski, G. A. Voth, P. Salvador, J. J. Dannenberg, S. Dapprich, A. D. Daniels, O. Farkas, J. B. Foresman, J. V. Ortiz, J. Cioslowski, and D. J. Fox, Gaussian, Inc., Wallingford CT, 2009. Gaussian 09 Revision A.02, Gaussian Inc. Wallingford CT 2009.
65 A. D. Becke, *Phys. Rev. A*, 1988, **38**, 3098-3100.
66 C. Lee, W. Yang and R. G. Parr, *Phys. Rev. B*, 1988, **37**, 785-789.
67 H. Naz, E. Jameel, N. Hoda, A. Shandilya, P. Khan, A. Islam, F. Ahmad, B. Jayaram and I. Hassan, *Bioorg. Med. Chem. Lett.* 2016, **26**, 782-788.

View Article Online
DOI: 10.1039/C8NJ03316A

Facile synthesis of triphenylamine and phenothiazine based Schiff bases for aggregation induced enhanced emission, white light generation, and highly selective and sensitive copper (II) sensing

Vivek Anand, Balaji Sadhasivam and Raghavachari Dhamodharan*

Graphical Abstract